JOURNAL OF GEOPHYSICAL RESEARCH, VOL. 101, NO. D6, PAGES 10,287–10,297, APRIL 30, 1996

Stratospheric temperature measurements by two collocated NDSC lidars during UARS validation campaign

Upendra N. Singh,[1] Philippe Keckhut,[2] Thomas J. McGee,[3] Michael R. Gross,[1] Alain Hauchecorne,[2] Evan F. Fishbein,[4] Joe W. Waters,[4] John C. Gille,[5] Aidan E. Roche,[6] and James M. Russell III [7]

Abstract. The NASA Goddard Space Flight Center (GSFC) mobile lidar system was deployed at the Observatoire de Haute Provence (OHP), during an Upper Atmosphere Research Satellite (UARS)/ Network for Detection of Stratospheric Change (NDSC) correlative measurement campaign (July-August 1992). The objective of this campaign was twofold: to intercompare two independent lidars and to provide ground-based UARS correlative ozone and temperature validation measurements. This paper, for the first time, presents a coincident temperature intercomparison between two independently operating temperature lidar systems of similar capabilities. Systems and retrieval algorithms have been described and discussed in terms of error sources. The comparison of the two analysis have shown very similar results up to the upper mesosphere. The statistical mean differences of 0.5 K in the stratosphere and about 2 K in the mesosphere suggests insignificant bias throughout except below 35 km, where one of the data sets is contaminated by the volcanic aerosols from the eruption of Mount Pinatubo. Profiles of the root-mean-square (RMS) of the differences are in good agreement with random error estimates, except around 35-40 km where RMS is larger. These measurements can be used as the ground reference for UARS temperature validation. However, the spatial-temporal coincidence between satellite and lidar needs to be carefully considered for meaningful validation.

1. Introduction

The idea for establishing a network of high-quality, remote sounding research stations for observing and understanding the anthropogenic changes in the stratosphere and any long-term impact on the Earth's atmosphere was first discussed at a workshop in 1986. In the following years, new instruments were developed and permanent sites were established. In January 1991 the international Network for Detection of Stratospheric Change (NDSC) [*Kurylo and Soloman,* 1990] became operational. To provide the best latitude coverage possible, it was proposed that the network would consist of at least seven stations: midlatitude, polar, and tropical, one in each hemisphere, and one near the equator. Each of the primary NDSC stations will be equipped with a large range of instruments to provide collocated measurements of most of the parameters and chemical species involved in stratospheric ozone chemistry. Depending on specific site characteristics such as geography or meteorology, a composite station may be formed with individual or groups of instruments at different sites within a given latitudinal or regional zone. Instruments were selected on the basis of being remote sensors, capable of continuous, long-term field operation. The homogeneity of such a network will be insured by continuous calibration and validation campaigns. Satellite sensors can be used as transfer references, as can high-quality, mobile instruments. One of the key measurements planned within the NDSC, along with ozone concentration, is the continuous monitoring of temperature in the middle atmosphere. Temperature monitoring is important, as temperature controls the rates of chemical reaction and thus ozone abundance. In addition, the temperature structure of the stratosphere itself is controlled by the ozone distribution. Stratospheric temperature change also occurs with increasing amount of carbon dioxide in the atmosphere. In general, the dynamical state of the middle atmosphere can be predicted by continually monitoring the temperature, as temperature is the combined manifestation of the dynamical, radiative, and chemical processes occurring in the middle atmosphere.

In recent years, several Rayleigh lidar systems have shown the technique to be a well-adapted method to measure stratospheric and mesospheric density and temperature [*Kent and Wright,* 1970; *Hauchecorne and Chanin,* 1980; *Chanin and Hauchecorne,* 1981, 1984; *Shibata et al.,* 1986; *Jenkins et al.,* 1987; *Philbrick et al.,* 1987; *Gobbi et*

[1]Hughes STX Corporation, Lanham, Maryland.
[2]Service d'Aeronomie, CNRS, Verrières-le-Buisson, France.
[3]Laboratory for Atmospheres, NASA Goddard Space Flight Center, Greenbelt, Maryland.
[4]Jet Propulsion Laboratory, Pasadena, California.
[5]National Center for Atmospheric Research, Boulder, Colorado.
[6]Lockheed Palo Alto Research Laboratory, Palo Alto, California.
[7]NASA Langley Research Center, Hampton, Virginia.

Paper number 96JD00516.
0148-0227/96/96JD-00516$05.00

al., 1988; *Dao et al.*, 1989; *Carswell et al.*, 1991; *Keckhut et al.*, 1993; *Meriwether et al.*, 1994; *Wickwar et al.*, 1995; *Whiteway and Carswell*, 1994, 1995; *Whiteway et al.*, 1995; *Ferrare et al.*, 1995] . The Observatoire de Haute Provence (OHP) in southern France is part of one of the first operational NDSC sites composing the northern midlatitude station (44°N, 6°E) "Alpine station." A permanent Rayleigh lidar system based at OHP was developed by Centre Nationale de Researche Scientifique - Service d'Aeronomie (CNRS) in 1979. The CNRS lidar system has been used routinely to obtain nighttime density and temperature profiles in the 30 to 80-km altitude range. Routine lidar observations of temperature since 1979 at OHP provide a large database to study the mesoscale variability of the middle atmosphere. These extended measurements have been used to study a wide range of geophysical phenomena, such as gravity and tidal waves, and the long-term trend analysis [*Chanin and Hauchecorne*, 1987; *Aikin et al.*, 1991; *Gille et al.*, 1991; *Hauchecorne et al.*, 1991; *Keckhut et al.*, 1995].

The accuracy of the Rayleigh lidar technique can further be improved through a better understanding of the sources of error. This can be accomplished by conducting intercomparison campaigns involving other instruments of similar capability and accuracy [*Keckhut et al.*, 1993]. Detection of sources of error and validation is not always possible due to lack of instruments of comparable accuracy and ability: Rocketsondes have sometimes shown poor repeatability [*Schmidlin*, 1981]; the falling sphere is affected by vertical winds below 45 km [*Schmidlin et al.*, 1991]; satellite sensors provide poor vertical resolution [*Remsberg*, 1986; *Aikin et al.*, 1991]; and balloon-borne radiosondes can present large uncertainties in determining the geometrical altitude around 30 km [*Nash and Schmidlin*, 1987]. One possible solution for further validation consists of comparing simultaneous temperature profiles obtained by two collocated independent lidar systems of comparable capabilities and accuracies. Such a validation campaign was possible with the deployment of the GSFC mobile lidar to OHP, during a UARS/NDSC correlative measurement campaign (JulyAugust 1992). While it was designed primarily for the measurement of stratospheric ozone, this lidar is also used to measure temperature and density using the Rayleigh lidar return of the reference channel [*McGee et al.*, 1991; *Ferrare et al.*, 1995].

In this intercomparison we have only considered lidar data which were collected coincident in time. This is particularly important if one wants to be sure that observed discrepancies, if any, are not the result of temperature change due to atmospheric changes. To better understand the sources of discrepancies, results are discussed in terms of the system characteristics and analysis techniques employed by the two groups.

To extend our knowledge of natural and anthropogenic variability to a more global scale, satellite measurements are necessary. High-quality measurements by ground-based lidars can provide an independent calibration of satellite sensors. Three-dimensional stratospheric temperature maps provided by National Meteorological Center (NMC) need ground reference to make adjustments to the temperature measurements obtained through the series of operational NOAA satellites. Lidar is proving to be an ideal candidate to replace rocketsondes, which were used in the past by NMC [*Finger et al.*, 1993]. Lidar temperature measurements have already been used extensively to validate temperature profiles obtained by the various temperature measuring instruments such as Microwave Limb Sounder (MLS), cryogenic limb array etalon spectrometer (CLAES), and Halogen Occultation Experiment (HALOE) [*Hervig et al.*, this issue; Fishbein et al., this issue; *Gille et al.*, this issue] aboard UARS [*Waters*, 1993; *Gille et al.*,1994; *Russell et al.*, 1994].

This paper compares two NDSC lidar instruments, their respective analysis software to derive the temperature profiles, measurement accuracies, and sources for small discrepancies observed between the two measurements. This paper also presents some near-coincident (spatial and temporal) temperature intercomparisons between the lidar and the UARS instruments to illustrate the potential of lidar, as a ground-based instrument, for validating satellite temperature measurements.

2. General Discussion of Experiment and Instruments

The GSFC mobile lidar was deployed to OHP, during a UARS/NDSC correlative measurement campaign (July-August 1992). The generator-powered lidar system is housed in a 45-foot trailer. The GSFC lidar system, designed primarily for measuring stratospheric ozone using the differential absorption lidar (DIAL) technique, has undergone several modifications and improvements in recent years [*McGee et al.*, 1991, 1993, 1995]. A XeCl excimer laser provides radiation at 307.9 nm, which is absorbed by ozone, and a XeF laser emitting at 351 nm is used as the atmospheric reference. Used together, these wavelengths permit the extraction of ozone profiles between 15 and 50 km. The Rayleigh return at 351 nm, alone, can be processed to derive temperature and density profiles between 30 and 70 km. The elastic return along with two additional N_2-Raman scattering returns can be used for computing aerosol scattering ratio, aerosol backscatter, and aerosol extinction profiles. When the aerosol layer approaches the background levels, the Raman backscattering signal can also be used to retrieve the temperature down to 10 km. The details of the system modifications, improvements, and capabilities are described by *McGee et al.*, [1995].

The CNRS Rayleigh lidar system measures stratospheric temperature and has also undergone several modifications since its inception [*Hauchecorne and Chanin* 1981; *Keckhut et al.*, 1993]. The lidar uses the second harmonic of a Nd:YAG laser for the temperature measurement. The system has been described in detail previously [*Keckhut et al.*, 1993]. A schematic of the relevant sections of both instruments deployed at OHP is given in Figure 1, showing the differences and similarities of the instruments. Table 1 compares the main characteristics of the two systems. Considering the wavelength dependence of the Rayleigh backscattering cross section, atmospheric transmission, and photomultiplier tube (PMT) quantum efficiency, the optimum spectral region for Rayleigh temperature lidar operation is 0.36-0.41 mm. The CNRS system uses the 532 nm wavelength mainly because of its low maintenance, high power, and long term reliability offered by the Nd:YAG

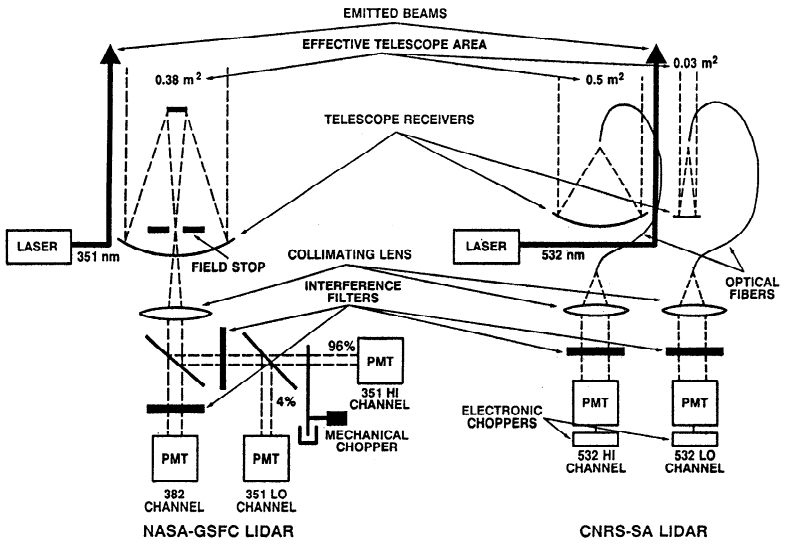

Figure 1. Schematic of the transmitter, receiver, and detector of GSFC and CNRS lidar systems during the UARS/Network for Detection of Stratospheric Change (NDSC) temperature intercomparison campaign at Observatoire d'Haute Provence (OHP), France.

lasers. The atmospheric extinction due to molecular scattering and absorption by ozone is also very small in the altitude range from 30 to 100 km (0.5%). Compared to the 532 nm, 351 nm is less sensitive to Mie scattering from aerosols, however, for both wavelengths, the validated temperature profile starts above the aerosol layer. During this campaign, aerosols from the eruption of Mount Pinatubo were still present in large amounts. Because temperature is usually extracted from a relative measure of the atmospheric density as measured by elastic scattering returns, any deviation from purely molecular scattering introduces an error into the temperature retrieval. This limits accurate temperature profiles to altitudes where aerosol scattering is negligible or about 35 km during these measurements. The vibrational Raman scattering at 382 nm from molecular nitrogen, collected by GSFC, has no contribution from aerosol backscattering and only a small signature from aerosol extinction. During this campaign at OHP, with heavy aerosol loading, the Raman signals were used successfully by GSFC to extend the temperature profile down to 27 km. The group at CNRS has also developed temperature measuring capabilities using vibrational-Raman [*Keckhut et al.*, 1990] and rotational-Raman [*Hauchecorne et al.*, 1992] techniques. Unfortunately, during this campaign these measurements were not available. A lower stratosphere temperature measurement, using Raman data, has been planned for future NDSC measurements.

Table 1. Lidar Characteristics

	CNRS	GSFC
	Transmitter	
Laser type	Nd:YAG	XeCl, XeF
Transmitted wavelengths, nm	532	308, 351
Pulse energy, mJ/pulse	350	250, 125
Repetition rate, Hz	50	50
Pulse width, ns	5-10	10-20
Emitted beam divergence, mrad	$4x10^{-2}$	0.5-1.0
	Receiver	
Detected wavelengths, nm		
elastic return	532	308, 351
Raman return		332, 382
Effective telescope area		
high channel, m^2	0.50	0.38
low channel, m^2	0.03	0.38
Field of View		
high channel, mrad	$2.5x10^{-1}$	2.3
low channel, mrad	0.55	2.3
Emitter-receiver distance, m		
high Channel	0.6	0.7
low Channel	0.3	0.7
Band-pass filter, nm	1.0	5.0
Ratio upper/lower sensitivity	20	24
Wavelength-corrected power aperture, $W\text{-}m^2$ (relative to 351 nm)	1.66	2.38

The receiver system used by the GSFC and CNRS differs considerably in design and concept. The GSFC uses a single 76-cm, Dall-Kirkham design with a variable aperture and can be operated between 0.1 and 2.3 mrad field of view. During this campaign the GSFC system operated in a quasi-coaxial configuration, with a separation of 0.7 m between the transmitted beam and the telescope. As indicated in the schematic (Figure 1), the temperature-measuring section of the GSFC lidar detector system consists of three channels: one collecting N_2-Raman scattering return at 382 nm and two additional Rayleigh channels. A beamsplitter was used to separate the Raman returns from the Rayleigh returns. To extend the dynamic range of the detectors, the GSFC system uses a beamsplitter (96-4%) to direct the incoming radiation to two different photomultiplier tubes of similar gain. The 4% channel (low) is used to collect the signals from the lower altitudes (15-40 km), whereas the 96% channel (high) collects returns from higher altitudes (25-90 km). The laser beam divergence of the GSFC system is of the order of 0.5 mrad, and since the laser system resides in a mobile trailer whose optical stability is not so optimum as the permanently

installed system, the field of view of GSFC is typically set to about 2 mrad. An interference filter of 5 nm was used in both Raman and Rayleigh channels to filter the broadband sky background. A desirable narrower linewidth filter could not be used because of the inherently broadband emission (348-353 nm) from the XeF laser [*Burris and Heaps,* 1995].

The CNRS system is also a quasi-coaxial system (0.6 m) but uses two separate telescopes, instead of a beam-splitter, to extend the dynamic range of the detectors. The smaller telescope (20 cm) has an effective area of 0.03 m^2, which is 6% of the large telescope, and is used as the low channel. The CNRS lidar uses an afocal system to transmit the laser beam in the atmosphere. This reduces the beam divergence by a factor of 10-15, to 0.04 mrad, and that permits CNRS system to set the field of view at 0.25 and 0.55 mrad, respectively, for high and low channel. Because of the narrow linewidth of the Nd:YAG laser output at 532 nm the CNRS lidar system uses an interference filter of 1-nm bandwidth to reduce the sky background. The use of narrow field of view of the telescope and a narrow bandwidth interference filter by the CNRS system results in significant reduction in sky background. This improves the signal-to-noise ratio (SNR) at high altitudes, which extends upward the altitude to which accurate temperatures can be derived. The CNRS system uses optical fibers to collect the backscattered photons at the focal point of the telescope and then directs them to the photomultiplier, which is generally located much farther away from the telescope. This provides better mechanical and thermal stability to the detector system.

Both systems, because of the difference in their configuration, utilize different techniques to align the transmitted laser beam to the field of view of the telescope [*McGee et al.,* 1995; *Keckhut et al.,* 1993]. The GSFC lidar system uses the signal collected between 30 and 35 km for alignment. A computerized, motor controlled mirror mount is used to sweep the beam through the field of view of the telescope, along four axes. The centroid is computed from these data and the beam is positioned at the center of the field of view of the telescope.

Since CNRS lidar uses two telescopes, the beam alignment with respect to the telescope is performed in a different fashion. Firstly, a smaller field of view is selected for the alignment of the high channel (larger telescope). The alignment is performed by optimizing the signal of the high channel by sweeping the beam through the field of view of the telescope. The alignment is more rigorous and critical because of smaller field of view. Once the alignment of the high channel is complete, the laser beam position becomes fixed and can not be moved for aligning the smaller telescope. A larger field of view, compared to the large telescope, is then chosen and then low channel return is optimized by moving the small telescope. The large field of view of the telescope makes it easier to align the smaller telescope to the transmitted beam. The quality of the alignment can be checked by taking the ratio of the number of photons in the common operating zone (40-70 km) of the two channels. For a proper alignment this ratio should be constant through the entire common altitude range [*Keckhut et al.,* 1993].

The GSFC and CNRS lidars were stationed 300 m apart. During the campaign period the GSFC and the CNRS lidar acquired 24 and 23 temperature profiles, respectively, of which 18 were coincident in time. The typical acquisition time for OHP lidar was about 7 hours, compared to about 3 hours for the GSFC lidar. The operation of another permanent lidar at OHP, this one measuring ozone on a routine basis, limited the GSFC lidar operation time to 3 hours. The CNRS temperature lidar transmitted 532 nm, a wavelength not detected by the GSFC lidars, so that both instruments could operate simultaneously. For the coincident intercomparison the raw data of CNRS lidar were selected to match the exact period of GSFC lidar acquisition. Since the state of the atmosphere is same during the coincident lidar observations by two systems, one can rule out geophysical phenomena, such as gravity waves, tides, etc., as being responsible for observed discrepancies, if any, between the two lidar measurements.

3. Linearity of the Detectors

In order for a Rayleigh lidar to get meaningful returns at high altitudes, it is necessary to transmit a large numbers of photons (high powered lasers) and to have a reasonably large telescope. This combination results in signals which vary over more than 6 orders of magnitude. Because of these factors, two types of nonlinearities can arise in the return signals, both of which are related to the large burst of photons from low altitudes. Signals from low altitudes are so large that the photomultiplier/amplifier/discriminator chain cannot count the pulses fast enough; the recorded signals are smaller than the actual. This type of nonlinearity can be referred to as pulse pileup [*Donovon et al.,* 1993]. In addition, when the photocathode of the photomultiplier is exposed to such large light levels, a long-lived decay is induced in the PMT output [*McGee et al.,* 1991]. This decay is evident in the background region of the lidar return, and it prevents an accurate determination of the ambient light level. It is then difficult to retrieve accurate lidar backscatter returns at high altitudes. This type of nonlinearity is often referred to as signal-induced noise (SIN). These two regions of nonlinearity are treated differently by each of the two groups in this work.

Nonlinearity in Pulse Counting

The GSFC instrument uses a beamsplitter (96-4%) and two detectors to collect elastically backscattered radiation. The beam was transmitted in a quasi-coaxial fashion and both channels were electronically gated up to 6 km. Even with two channels, the limited band pass of the counting system leads to pulse-pile effects at low altitudes. When a large number of photons reach the photocathode, there is a high probability of two or more photoelectrons being emitted spaced closely enough in time that the detection system cannot resolve them. The minimum time by which two pulses from the detector must be separated in order that both be counted, i.e., the dead time, is influenced by the bandwidth of the both the amplifier and the discriminator. Depending on the detection system, different expressions can be used to correct these nonlinear effects.

The GSFC system uses a non-extending type detection/discrimination system for photon counting [*Funck,* 1986]. The observed average rate of the event occurrences will asymptotically tend toward a maximum average

observed count rate equal to the inverse of the resolving time and requires a correction of the following form:

$$N = \frac{n}{(1 - nr)} \quad (1)$$

where N is the true number of counts, n is the measured number of counts , and r is the resolving time of the instrument. The resolving time is measured for both channels, by recording the backscatter return with an attenuation between 10 and 100 and comparing it to the full strength return.

The CNRS uses an extending type detection/discrimination system for photon counting. This system response tends toward zero if the frequency of events is large enough. The true number of counts can be computed by using the following expression [*Funck*, 1986]:

$$N_{count} = N_{received} \exp(- \frac{N_{received}}{N_{max}}) \quad (2)$$

where N_{max} is the parameter which characterizes the detection system and corresponds to the maximum numbers of photons it can count and is measured a priori. This correction is used systematically for the low channel.

A wrong setting of the discriminator threshold can induce nonlinearity in the photon counting, as per pulse-pileup effect [*Donovan et al.*, 1993]. Such effects can be avoided by properly setting the discriminator level before acquiring the data. In an another approach, used by the CNRS, the channel dedicated for upper layers in the CNRS lidar uses a more sophisticated expression by adding a term of second order:

$$N_{count} = N_{received} \exp (- \frac{N_{received}}{N_{max}} - K N^2_{received}) \quad (3)$$

For this channel the correction is not performed with a priori values but is systematically determined for each night using a least squares fit method and linking both channels through the above function. Both coefficient N_{max} and K are determined by fitting the corrected low-channel signal (N_{count}) with the high channel signal ($N_{received}$) in the overlap region (35-55 km) using equation (3). A continuous signal is constructed using the low channel for altitude less than 35 km, the high channels above 45 km, and a composite signal for both channels at altitude between 35 and 45 km. A weighing function is used for smooth transition between 35 to 45 km.

Signal-Induced Noise

Major modifications were incorporated in the GSFC lidar system before the OHP campaign to completely eliminate signal-induced noise (SIN) in the most sensitive channels. A detailed description of the severity of the SIN problem and effect of implemented modifications are given by *McGee et. al.* [1995]. Mechanical choppers were placed in front of the high-sensitivity 308- and 351-nm channels to physically block the photocathode from backscattered radiation when the laser beams are in the lower atmosphere. A test was conducted at the beginning of the campaign at OHP, France [*McGee et al.*, 1995]. The test result showed that without the mechanical chopper blocking the initial lidar return, the background region between 90 and 175 km for the 351-nm high-sensitivity channel was nonlinear and had a definite negative slope. When the chopper is operated, the background region of the return signal is flat, and the magnitude of the region has been reduced by as much as a factor of 5. In all cases during the OHP campaign, a mean background fit for the high channel was used.

It was observed during the OHP campaign that the lidar returns in the low channel exhibited some SIN. This occurred, even though the PMT was electronically gated off until the beam had traveled 6 km. The effect of this SIN was evident at the high end of the retrieved temperature profiles from the low channels at altitudes above where the low-channel temperature was used in the composite temperature profile. It was negligible at the altitudes which were used in the profile.

As mentioned before, the CNRS lidar employs two independent telescopes of different sizes to extend the dynamic range. The smaller telescope's effective telescope area is 0.03 m^2, compared to 0.5 m^2 for the large telescope. Electronic gates is used on each channel, in an effort to reduce the effects of the large initial burst of light. The time delay for the gating is adjusted each day depending on the atmospheric transmission, laser power, and strength of the backscattered return. The gating is turned off at approximately 15-20 km. This results in reducing the signal-induced noise in the low channel, but as the mean level of the background noise is small, a small residual SIN can be identified. Fitting routines are used to estimate the background, which is then extrapolated back into the data in an effort to remove the effects of signal-induced noise.

For the high channel, a separate electronic gate, independent of the low channel, is used in the CNRS lidar to handle the high altitude nonlinearities resulting from SIN. The use of electronic gate is not so ideal a solution as using a mechanical chopper. The reason being, a mechanical chopper physically blocks the light from hitting the photocathode, but the gated PMT does not. Thus some transient effects can be observed when gates are turned on. These effects are not longer than a few microseconds in the case of the CNRS system and does not effect the range of the measurement considerably. Time delays as large as 13 to 17 μs are usually used. As a result, the signal-induced noise is considerably reduced but still can be identified from the very low mean background noise. To estimate the signal-induced noise, a model backscattered signal is constructed by normalizing the CIRA 86 model to the experimental data at 40 km. By subtracting this model backscattered signal from the real backscattered signal, a first estimate of the SIN is obtained. For the altitude range where the backscattered signal is small compared to the noise (>90 km), a quadratic fit of the estimated noise is calculated from the altitude where the statistical noise is equal to 15% ($\sqrt{n}/n = 0.15$) up to the end of collected data. This quadratic function is then extrapolated back to lower altitudes and subtracted from the data.

4. Algorithm

Middle atmospheric density and temperature profiles are derived from the Rayleigh backscattering of a monochromatic laser pulse by air molecules. The methodology was first suggested by *Elterman*, [1953] and further developed by *Hauchecorne and Chanin*, [1980]. With slight variation this method has been adapted by both GSFC and CNRS

[*Ferrare et al.*, 1995; *Keckhut et al.*, 1993]. As the relative density of the atmosphere is directly related to the backscattered signal, first a relative density profile is computed. The temperature profile in decreasing altitude is then derived from the computed relative density profile using the hydrostatic equation and the ideal gas law. A reference pressure at the top of the profile is estimated from an atmospheric model. However, because of the exponential decrease of the pressure the influence of any error in pressure estimation rapidly becomes negligible within 5-10 km of the top altitude and an absolute temperature measurement can be obtained.

Data, from which temperature profiles are derived, are the sum of the lidar returns from a large number of laser shots over the course of a night operation. The temporal and vertical resolutions, along with the number of photons received in a designated range bin, determine the precision of the measurement. The accuracy of the computed temperatures depends on the shot noise of the returned signal. This is improved by increasing the integration time and by degrading the vertical resolution, when looking at long-term varying processes. Several hours and several hundred meters are usually the parameters used with lidar. The measurements derived from lidar data then represent a mean temperature during these integration times and for a layer of thickness determined by the vertical resolution. During this campaign the maximum vertical resolution of GSFC and CNRS was 150 and 300 m, respectively. For each measurement the resolution was degraded to improve the precision. For the GSFC system the typical range resolution was between 1 and 7 km, and for the CNRS it was 3 km.

A detailed description of the error sources is first given by *Hauchecorne and Chanin* [1981]. However, considering the inherent differences between the two systems, specific technical aspects of both systems are compared and analysis algorithms discussed.

Initialization

As mentioned before, temperature profiles are obtained from relative density profiles. Computation of the temperature profile requires a pressure initialization at the top of the profile. To initialize the pressure profile, it is assumed that the values of this parameter at the top of the profile (i.e., for the last 10 km) are, on average, equal to those of the standard atmospheric model. The calculation of uncertainty due to this normalization shows that this error (in pressure estimation) becomes negligible within approximately 20 km due to the exponential decrease in the atmospheric pressure. Statistical noise, however, increases with altitude [*Keckhut et al.*, 1993]. Therefore the temperature obtained, even with this pressure initialization, can be considered absolute and the estimated error consists mainly of the photon noise. However, the differences in the analysis method and the quality of the model used (U. S. Standard, CIRA 76, CIRA 86, CIRA 90) could introduce some systematic bias between the mesospheric temperature measurements by the two analyses. Even if the statistical noise is sufficiently large to overcome the possible differences, it is important to improve such procedures to accurately compute the temperature in the mesosphere for long-term analysis.

The procedure used for the pressure initialization is straightforward. For temperature computation the density profile is measured up to the nth layer. The pressure in the ith layer is calculated from the integration of the density profile in assuming an initialized pressure P_i as follows:

$$P\left(z_i+\frac{dz}{2}\right) = \int_{j=i+1}^{n_{top}} \rho(z_j)g(z_i)dz + P_i\left(z_{n_{top}}+\frac{dz}{2}\right) \qquad (4)$$

where ρ (z) is the density and g (z) is the acceleration of gravity. To initialize the pressure profile, we assume that the values of this parameter at the top of the profile are, on average, equal to those of the standard atmosphere model for the corresponding month, latitude, and altitude layer (CIRA 86).

The GSFC uses the CIRA 86 atmospheric model and initialization of the pressure profile is done at a point where statistical noise is equal to 5% in a single 150-m range cell. As relative pressure changes at 80-90 km are observed to be twice than those observed in temperature at these altitudes, the CNRS uses a different method in their analysis.

From equation (4), and integrating the density for a 10-km layer below the top of the profile, and using the differential pressure from the top and the bottom layers, the initialized pressure can be calculated as follows:

$$P_i(z_{n_{top}}+dz/2) = \frac{P_m(z_{n_{top}}+dz/2)}{P_m(z_{n_{bot}}+dz/2)-P_m(z_{n_{top}}+dz/2)} \times \int_{n_{bot}+1}^{n_{top}+1} \rho(z_j)g(z_j)dz \qquad (5)$$

This process of initialization is based on a pressure ratio obtained from the model and it can be considered equivalent to a direct temperature initialization. Although it uses a pressure model, this procedure adjusts both the model and the observed scale height, which is directly related to temperature. The CNRS analysis have also used the CIRA 86 model, which includes seasonal and horizontal dimensions, to initialize the pressure at a level where statistical noise is equal to 15% for the 1-km-smoothed profile. The GSFC criterion is considerably more stringent. As the initialization is based on the signal integration over a 10-km layer, it is less sensitive to waves than the single point initialization. Recent studies have demonstrated discrepancies in the mesosphere between the measured temperature and the one given by the CIRA 86 model [*She et al.*, 1993]. Here it is not our purpose to discuss the validity of the measurement in the mesosphere, however some improvements on the initialization process could be performed in the future by using some improved mesospheric model.

Smoothing

As the filtering process is important in retrieving lidar-derived ozone profiles, the GSFC temperature analysis has used the same sophisticated filter (nearly equal ripple low-pass filter) for data smoothing. Since the random error in the lidar signal increases with altitude, the vertical resolution of this smoothing filter increases with altitude to reduce error in the derived temperatures. The vertical resolution from 30 to 70 km ranges from 1 to 7 km, respectively. The algorithm was tested for its ability to preserve periodic temperature variations. However, where the resolution of the smoothing filter becomes comparable or larger than the wavelength of

the temperature waves, the amplitude of the perturbations are largely underestimated. So in the upper stratosphere (30-50 km), more wave structures are observed in the GSFC analysis as compared to the CNRS analysis. In the CNRS analysis a constant vertical filtering is applied by using a low-pass Hanning filter. This analysis maintains a vertical homogeneity, with respect to wave frequency, by uniformly smoothing any vertical temperature perturbations of wavelengths smaller than 3 km.

Algorithm Comparison

The algorithms developed by both groups for deriving density and temperature profiles from the Rayleigh backscatter return are based on the methodology first described by *Hauchecorne and Chanin* [1980]. Although the basic principles and assumption of the initial technique remained the same, pertaining to their transmitter and detector system differences, the analysis algorithms adapted by both groups for temperature derivation differ in certain areas. Thus it is essential to compare the two analysis algorithms to rule out any systematic bias arising due to difference in the algorithms.

To this end, several raw data set obtained by the GSFC lidar were analyzed using the independently developed algorithms of two groups. The comparison of the retrieved temperature profiles from both analyses have shown very good agreement and differences remain within the ±1 σ statistical error bars, as seen on July 31, 1992 (Figure 2). The errors seem to be well estimated. In the upper mesosphere where the largest differences are observed, the errors are apparently mainly due to the effect of the initialization. As described before, this discrepancy comes from the different altitude of initialization and the different noise extraction process used in the two algorithms. This part of the profile is the only area where differences are evident, and there are no ancillary measurements available at these altitudes to validate the profiles. A recent comparison between the CNRS lidar at OHP and a sodium lidar measurement made at a similar latitude at Fort Collins, Colorado, has shown very good agreement [*She et al.*, 1995]. However, collocated measurements are needed to be able to perform sensitivity studies of the initialization process. Results of algorithm intercomparison between this campaign and the other NDSC campaigns are being evaluated and efforts are under way to recommend a standard algorithm to be used for temperature extraction by all NDSC lidars.

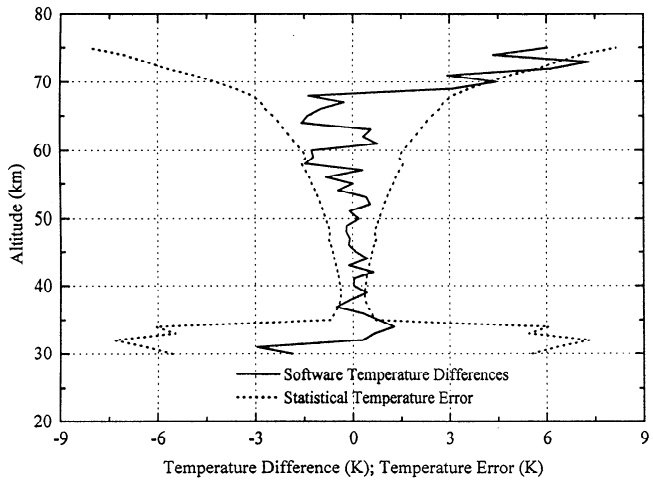

Figure 2. Profile of the percentage temperature difference between the same raw data (acquired by GSFC lidar on July 31, 1992) processed by the two algorithms (solid line). Differences is (algorithm CNRS- algorithm GSFC). Dotted lines indicate the square of the quadratic sum of the statistical error estimate by the two analysis softwares.

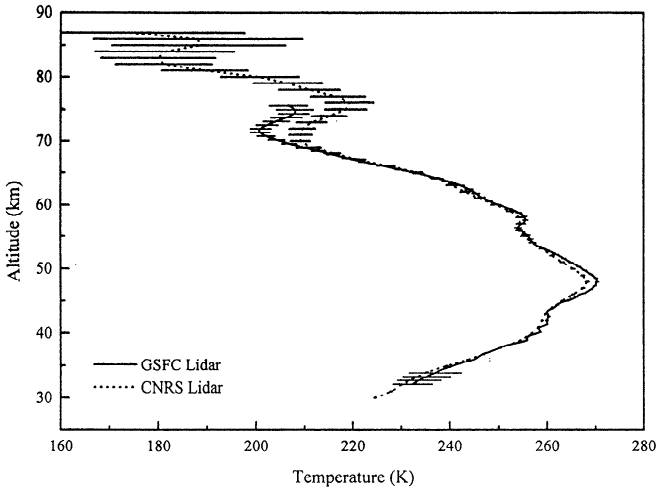

Figure 3. Comparison of the temperature profiles recorded simultaneously by GSFC (solid line) and CNRS (dotted line) lidars on August 4, 1992. Horizontal bars represent estimated errors for ±1 σ standard deviation.

5. Results and Discussions

Lidar Intercomparison

For the blind intercomparison, data were acquired, analyzed, and submitted in a routine manner without adjustments in the instrument or analysis algorithms. The data used for blind comparison included the entire night of CNRS lidar acquisition and about 3 hours of GSFC lidar acquisition. The operation of another permanent lidar at OHP, this one measuring ozone on a routine basis and operating at the same wavelength as the GSFC lidar, limited the GSFC lidar operation time to 3 hours. The CNRS temperature lidar transmitted 532-nm, a wavelength not detected by the GSFC lidars, so that both instruments could operate simultaneously. Although the general agreement between measurements made by each system is quite good, there exist some small discrepancies between the two measurements. One possible source for these discrepancies may be the different integration periods used for the blind comparison. It is important, for the detection of long-term changes, to understand even the small differences between the two measurements. The separation of errors into two classes, random and bias, is also important when absolute measurements over a long period are expected. As there exist some differences between both systems, it is interesting to see if the observed differences could be explained by our knowledge of the source of the errors involved.

For the blind intercomparison, only nights, when both lidars operated were considered (18 profiles). The blind

intercomparison indicated relative differences of GSFC temperature measurements with respect to the CNRS, for the whole campaign period (18 nights), less than 1% between 34 and 37 km (standard deviations within 2% at ± 1 sigma), and less than 2% up to 70 km (standard deviation up to 10% at ± 1σ) (P. Simon, personal communication, 1994).

The same data set, submitted for the blind comparison, are used here, except that the integration time of the CNRS data set was reduced to match the GSFC integration time. Figure 3 shows a typical coincident temperature profile intercomparison for August 4, 1992. Excellent agreement between the two profiles can be seen up to 68 km. Both lidars were able to capture highly correlated structures in the temperature profile. Large differences between the two profiles can be seen above 68 km. These obviously, as discussed before, are due to pressure initialization at different altitudes in the two algorithms. Lower in altitude the difference converges and disappears completely at 10 km below the top of the GSFC profile.

The average of the 18 coincident profiles from each instrument and the percentage difference of the averages are shown in Figure 4a. The error bars are the standard errors (standard deviations divided by the square root of the number of profiles). The difference of the averaged coincident profiles of the GSFC and the CNRS lidar is slightly better than the blind intercomparison performed with the full recorded data. Above 35 km altitude the CNRS temperatures are slightly colder than GSFC with an overall agreement better than 1.5% up to 75 km. Below 35 km altitude the CNRS temperature results are much colder than the GSFC ones, the largest differences being at the lower limit of the altitude range (3% at 30 km). This difference is due to the fact that the CNRS lidar operating at 532 nm is much more disturbed by the Pinatubo aerosol layer than the GSFC lidar, operating at 351 nm. Also, the GSFC system uses Raman channels at 382 nm for its temperature extraction at lower altitudes. Raman returns are much less perturbed by heavy aerosol loading from volcanic eruptions.

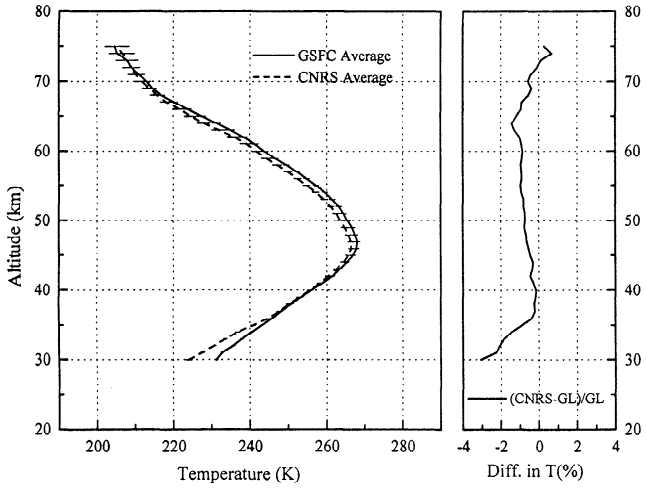

Figure 4a. (Left) Average of 18 coincident temperature profiles from each instrument (solid line, GSFC; dotted line, CNRS). (Right) Percentage temperature difference between the average CNRS and the GSFC coincident profiles. Error bars in the left plot represents the standard error.

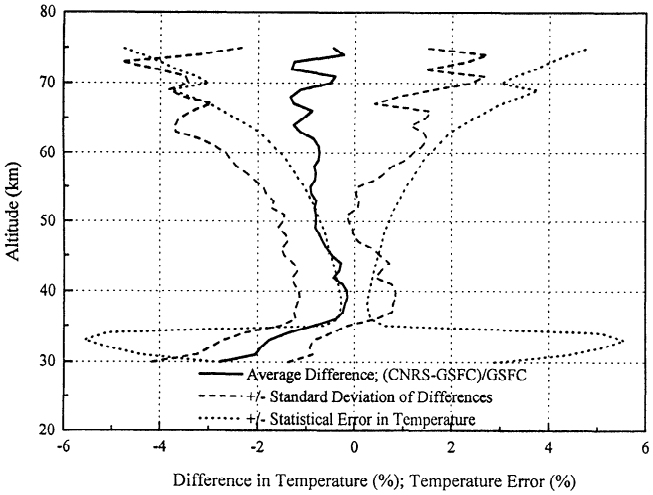

Figure 4b. Mean statistical difference of 18 coincident temperature profiles obtained by the two lidars. Solid line represents the mean relative temperature difference between the two lidars (CNRS-GSFC)/GSFC. Root-mean-square of the difference is indicated by dashed line and the mean square of the quadratic sum of the statistical error estimates by the two lidars is represented by dotted line.

For a better understanding of the differences and the errors involved, an average statistical difference of 18 coincident profiles from the two lidars is shown in Figure 4b. It is worth pointing out that the difference plot shown in Figure 4a is different from the one shown in Figure 4b. For this later plot, differences between two average profiles from two instruments were calculated for each individual day and were then averaged for 18 coincident days, whereas Figure 4a shows the difference between the average of two profiles, one from each instrument for all 18 coincident days. In the stratosphere the relative temperature differences between the GSFC and the CNRS lidars are less than 0.2% with standard deviations less than 2% at ± 1σ.

In the mesosphere the agreement between the two lidars is better than 1.5% up to 75 km, with standard deviation from 1.5 to 8% at ± 1σ. The oscillations observed in the mesosphere are probably caused by the different filtering processes used by the two groups, since the mean differences remain small in all these cases. In the GSFC analysis, temperature profiles are calculated independently for high- and low-sensitivity elastic returns, and the Raman returns. These are joined together to create a composite temperature profile. In the CNRS analysis a continuous signal from the high and low channels are formed after applying the saturation correction. The temperature is then calculated from this single corrected signal.

Random errors can be estimated by the root-mean-square (RMS) of the difference of the daily profiles. Some of these uncertainties are well known (e.g., shot noise and initialization errors) and are estimated for each measurement. These random errors are smaller than 0.4% around 35 km and about 1.5% and 5% in the lower and upper mesosphere, respectively. This shows quite a good agreement revealing a good estimate for the uncertainties of shot noise and initialization error. However, in the stratosphere, daily changes (2%) seem to be larger than estimates (0.4%).

Overlapping of both channels and small misalignment effects could be the source of such discrepancies. However, mean differences are insignificant and smaller than the random errors given by both noise estimates or the RMS of the daily differences. The difference of nearly 1% observed from the stratopause to the upper mesosphere is significant according to the standard error mainly around the stratopause.

We can conclude from this comparison that in the mesosphere the random error comes primarily from statistical counting, initialization, and filtering effects. In the stratosphere these errors are small (± 2.5 K). Investigations need to continue to understand the source of discrepancies and to improve the methods to bring the differences under the statistical noise (± 0.5 K in the stratosphere).

Satellite Validation

One of the primary goals of the NDSC is to provide accurate groundtruth measurement for satellite validation. The lidar data have been extensively used to validate temperature profiles obtained by UARS instruments [*Fishbein et al.*, this issue; *Hervig et al.*, this issue; *Gille et al.*, this issue]. Although it is not our main objective to present a complete satellite validation, some intercomparisons between lidar and UARS temperature profiles (MLS, CLAES, and HALOE) obtained during this campaign have been reported here to illustrate the correlation and potential of lidar instruments for validation of satellite measurements. Figure 5 presents such a comparison for a given day (August 9, 1992) when all three temperature-measuring instruments on UARS made close coincident measurements. The temperature differences, using the GSFC lidar as a reference reveal an overall agreement of 3%, with larger differences in the lower mesosphere and near the 2-mbar level (42 km). The agreement is better than 1% around

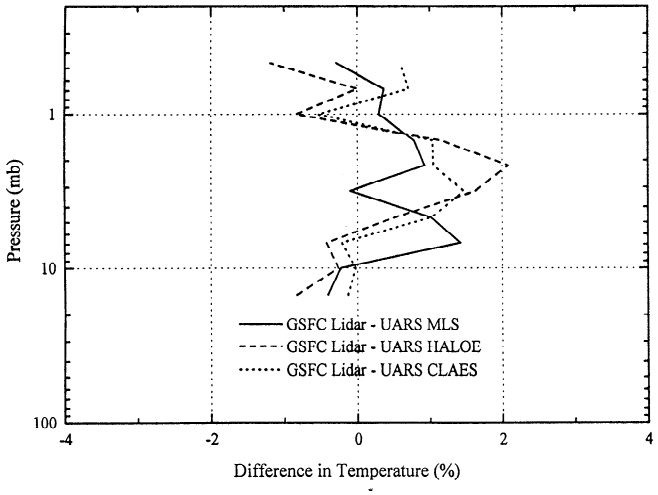

Figure 5. Percentage relative temperature difference between the near-coincident UARS (MLS, HALOE, and CLAES) and GSFC lidar profile recorded on August 9, 1992, over OHP. GSFC lidar data have been used as reference; percentage relative temperature differences with MLS, HALOE, and CLAES profiles between 22 mbar to 0.4 mbar are represented by solid, dashed, and dotted lines, respectively.

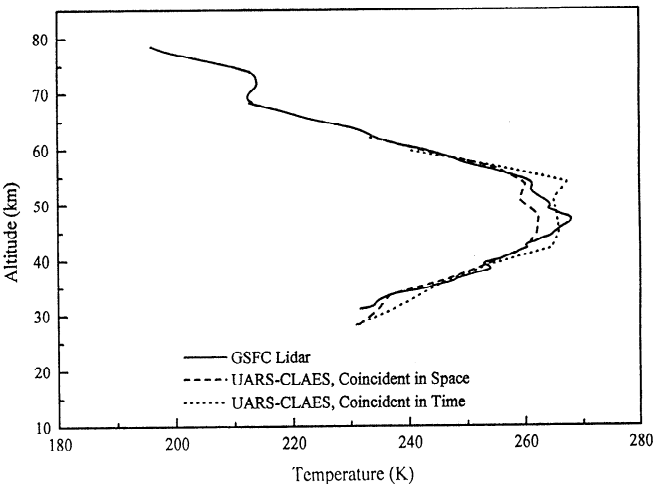

Figure 6. GSFC lidar temperature profile recorded on July 27, 1992 (solid line), is compared to the spatial near-coincident (dashed line) and temporal near-coincident (dotted line) temperature profile from UARS CLAES experiment.

the stratopause. The routine measurements performed by the lidar at OHP since 1979 [*Hauchecorne et al.*, 1991] have always observed quite small day-to-day variability at this level (<2 K). These lidar measurements have also revealed a larger variability around 40 km (3-4 K) and in the mesosphere, associated with the upper stratospheric warming and the induced mesospheric cooling. From April to October this variability is reduced down to 2-3 K in the middle stratosphere, mainly due to the blocking of planetary waves by strong easterly winds. However, a secondary minimum (3-4 K) is observed during July and could be explained by the propagation of short-period planetary waves. The reduced variability from April to October still exists in the lower mesosphere, but above 60 km the variability remains large and quickly increases with altitude due to the breaking of gravity waves. As the satellite measurements plotted here are not obtained simultaneously and strictly over the same site, the discrepancies could be interpreted as spatial and temporal geophysical effects. During July 27, two temperature profiles from the CLAES experiment onboard the UARS satellite were selected as the nearest in horizontal distance and time with the lidar and are compared in Figure 6. One can observe that the nearest spatially coincident profiles have similar structures but present large differences (~5 K) in the mean absolute temperature between 40 and 55 km. In contrast, the nearest temporally coincident profiles demonstrate good agreement for the temperature between 40 and 55 km, with slightly different shape. More statistical sampling of near-coincident lidar and UARS temperature profiles needed to be intercompared to see whether temporal or spatial coincidence should be considered for a validating UARS temperature profile. These issues and gravity and tidal wave effects are the topic of a forthcoming paper, where near-coincident temperature profile from MLS, CLAES, and HALOE for the period covering 1992-1995 will be intercompared with the results obtained by GSFC lidar. Lidar and UARS measurements have recently been used for studying the semidiurnal and diurnal tides in the stratosphere and mesosphere [*Keckhut et al.*, this issue].

6. Summary and Conclusions

The NDSC network was officially initiated in January 1991 and is still under development. Validation of the instruments located at different NDSC sites was planned to be accomplished by using existing collocated instruments at that site or by bringing mobile instruments from different sites and using them as reference to calibrate the instrument at the permanent site. Rayleigh lidar was chosen to provide vertical temperature profiles from 30 to 70 km. The GSFC system was deployed at the OHP site in the summer of 1992 for coincident temperature intercomparison with the CNRS lidar stationed permanently at OHP. A total of 18 coincident profiles were taken by both systems during the campaign. There exist some basic experimental differences between the two systems and they utilize slightly different algorithms for temperature derivation. Use of different initialization and filtering methods has been found to induce some differences in the temperature retrieval in the upper mesospheric part of the profiles. However, raw data processed through the two algorithms have indicated hardly any difference in the temperature profile starting in the middle stratosphere up to the middle mesosphere. The blind intercomparison of both data sets has shown quite good agreement. The statistical differences have revealed mean differences of 0.5 K in the stratosphere and less than 2 K in the mesosphere. Larger differences are observed below 35 km. This was primarily due to the presence of volcanic aerosols at those altitudes, and the fact that the 532-nm wavelength used by the CNRS lidar is much more sensitive to Mie scattering from the aerosol than the 351-nm wavelength used by the GSFC lidar. More importantly, the GSFC system has used a vibrational nitrogen-Raman channel to derive temperature at altitudes where aerosols are present. Profiles of the root mean square of the differences are in good agreement with the random error estimates (initialization and shot noise) except in the stratosphere around 35 km, where one can expect a random variability between data acquired and analyzed by the two groups to be about 1-2 K ($\pm 1\sigma$). Even though more investigations are needed to understand and to minimize such differences, this campaign revealed the great repeatability and potential of such temperature measurements available under the NDSC network. Satellite instruments can use these measurements as ground truth. However, the characteristics of satellite and lidar measurements makes strict coincidence in space and time very difficult to achieve. Some illustrations of such comparison have been shown. A more detailed near-coincident intercomparison is under way.

Acknowledgments. The authors would like to thank the staff at the Observatoire de Haute Provence, in St. Michel l'Observatoire, France, for their assistance and efforts while GSFC lidar was deployed there. The research and improvements have been funded by the NASA Upper Atmosphere Program and the Upper Atmosphere Research Satellite Correlative Measurements Program. Thanks are also due to SPA-AFEAS for providing travel funds to GSFC for the international campaigns.

References

Aikin, A. C., M. L. Chanin, J. Nash, and D.J. Kendig, Temperature trends in the lower mesosphere, *Geophys. Res. Lett., 18,* 416-419, 1991.

Burris, J., and W. Heaps, Temporal variations in the spectral output of a xenon fluoride excimer laser, *Appl. Opt., 34,* 426-427, 1995.

Carswell, A. I., S. R. Pal, W. Steinbrecht, J. A. Whiteway, A. Ulitsky, and T. Y. Wang, Lidar measurements of the middle atmosphere, *Can. J. Phys., 69,* 1076-1086, 1991.

Chanin, M. L., and A. Hauchecorne, Lidar studies of gravity and tidal waves in the stratosphere and mesosphere, *J. Geophys. Res., 86,* 9715-9721, 1981.

Chanin, M. L., and A. Hauchecorne, Lidar studies of temperature and density using Rayleigh scattering, *Map Hand., 13,* 87-99, 1984.

Chanin, M. L., and A. Hauchecorne, Long-term variation of the temperature of the middle atmosphere at midlatitude: Dynamical and radiative causes, *J. Geophys. Res., 92,* 10,933-10,941, 1987.

Dao, P., W. Klemetti, D. Sipler, W. P. Moskowitz, and G. Davidson, Density measurements with combined Raman-Rayleigh lidar, *Proc. SPIE Int. Soc. Opt. Eng., 1062,* 138-143, 1989.

Donovan, D. P., J. A. Whiteway, and A. I. Carswell, Correction for nonlinear photon-counting effects in lidar systems, *Appl. Opt., 32,* 6742-6753, 1993.

Elterman, L., A series of stratospheric temperature profiles obtained with the searchlight technique, *J. Geophys. Res., 58,* 519-530, 1953.

Ferrare, R. A., et al., Lidar measurement of stratospheric temperature during STOIC, *J. Geophys. Res., 100,* 9303-9312, 1995.

Finger, F. G., M. E. Gelman, J. D. Wild, M. L. Chanin, A. Hauchecorne, and A. J. Miller, Evaluation of NMC upper-stratospheric temperature analysis using rocketsonde and lidar data, *Bull. Am. Meteorol. Soc., 74(5),* 789-799, 1993.

Fishbein, E. F., et al., Validation of UARS Microwave Limb Sounder temperature and pressure measurements, *J. Geophys. Res.,* this issue.

Funck, E., Dead time effects from linear amplifiers and discriminators in single detector systems, *Nucl. Instrum. and Meth. Phys. Res., A245,* 519-524, 1986.

Gille, J., S. Massie, P. Bailey, A. Roche, J. Kumer, J. Mergenthaler, and L. Lyjak, Early results of validation and application of CLAES data, *Adv. Space Res., 14,* (9)-5-(9)-11, COSPAR, Pergamon Press, 1994.

Gille, J. C., et al., Accuracy and precision of cryogenic limb array etalon spectrometer (CLAES) temperature retrievals, *J. Geophys. Res.,* this issue.

Gille, S. T., A. Hauchecorne, and M. L. Chanin, Semidiurnal and diurnal tidal effects in the middle atmosphere as seen by Rayleigh lidar, *J. Geophys. Res., 96,* 7579-7587, 1991.

Gobbi, G. P., A. Adriani, F. Congeduti, and M. Viterbini, Lidar measurements of density and temperature in the middle atmosphere, paper presented at 14th International Laser Radar Conference, Innichen-San Candido, Italy, June 20-24, 1988.

Hauchecorne, A., and M. L. Chanin, Density and temperature profiles obtained by lidar between 30 and 70 km, *Geophys. Res. Lett., 7,* 564-568, 1980.

Hauchecorne, A., M. L. Chanin, and P. Keckhut, Climatology and trends of the middle atmospheric temperature (33-87 km) as seen by Rayleigh lidar over the south of France, *J. Geophys. Res., 96,* 15,297-15,309, 1991.

Hervig, M. E., et al., A validation of temperature measurements from the Halogen Occultation Experiment, *J. Geophys. Res,* this issue.

Jenkins, D. B., D. P. Wareing, L. Thomas, and D. Vaughan, Upper stratospheric and mesospheric temperatures derived from lidar observations at Aberystwyth, *J. Atmos. Terr. Phys., 49,* 287-298, 1987.

Keckhut, P., M. L. Chanin and A. Hauchecorne, Stratosphere temperature measurement using Raman lidar, *Appl. Opt., 29,* 5182-5186, 1990.

Keckhut, P., A. Hauchecorne and M. L. Chanin, A critical review on the data base acquired for the long term surveillance of the middle atmosphere by french Rayleigh lidars, *J. Atmos. Oceanic Technol., 10,* 850-867, 1993.

Keckhut, P., A. Hauchecorne, and M. L. Chanin, Midlatitude long-term variability of the middle atmosphere: Trends, cyclic and episodic changes, *J. Geophys. Res., 100,* 18,887-18,897, 1995.

Keckhut P., et al., Semidiurnal and diurnal temperature tides (30-55 km): Climatology and effect on UARS-lidar data comparison, *J. Geophys. Res.,* this issue.

Kent, G. S., and R. W. Wright, A review of laser radar measure-

ments of atmospheric properties, *J. Atmos. Terr. Phys., 32,* 917-943, 1970.
Kurylo, M. J., and S. Solomon, Network for the Detection of Stratospheric Change, *NASA Rep., Code EEU,* 1990.
McGee, T. J., D. Whiteman, R. Ferrare, J. J. Butler, J. F. Burris, STROZ LITE : Stratospheric ozone lidar experiment, *Opt. Eng, 30,* 31-39, 1991.
McGee, T. J., M. R. Gross, R. Ferrare, W. Heaps, and U. N. Singh, Raman DIAL measurements of stratospheric ozone in the presence of volcanic aerosols, *Geophys. Res. Lett., 20,* 955-958, 1993.
McGee, T. J., M. R. Gross, U. N. Singh, J. J. Butler, and P. E. Kimvilakani, Improved stratospheric ozone lidar, *Opt. Eng., 34,* 1421-1430, 1995.
Meriwether, J. W., P. D. Dao, R. T. McNutt, W. Klemetti, W. Moskowitz, and G. Davidson, Rayleigh lidar observations of mesospheric temperature structure, *J. Geophys. Res., 99,* 16,973-16,987, 1994.
Nash, J., and F. J. Schmidlin, Final report of the WMO international radiosonde intercomparison, *WMO Rep. 30,* 120 pp., Geneva, Switzerland, 1987.
Philbrick, C. R., D. P. Sipler, G. Davidson, and W. P. Maskowitz, Remote sensing of structure properties in middle atmosphere using lidar, in Topical Meeting on Laser and Optical Remote Sensing, pp. 120-123 , Opt. Soc. of Am., North Falmouth, Mass., Sept 28-Oct. 1, 1987.
Remsberg, E. E., The accuracy of Nimbus 7 LIMS temperature in the mesosphere, *Geophys. Res. Lett., 13,* 311-314, 1986.
Russell, J. M.,III, L. L. Gordley, L. E. Deaver, R. E. Thompson, and H. Park, An overview of the Halogen Occultation Experiment (HALOE) and preliminary results, *Adv. Space Res., 14,* (9)-13-(9)-20, COSPAR, Pergamon Press, 1994.
Schmidlin, F. J., Repeatability and measurement uncertainty of the United States meteorological rocketsonde, *J. Geophys. Res., 86,* 9599-9603, 1981.
Schmidlin, F. J., M. S. Lee, and W. Michael, The inflatable sphere: A technique for the accurate measurement of middle atmosphere temperatures, *J. Geophys. Res., 96,* 22,673-22, 682, 1991.
She, C. Y, J. R. Yu, and H. Chen, Observed thermal structure of the mid-latitude mesopause, *Geophys. Res. lett., 20,* 567-570, 1993.
She, C. Y., J. R. Yu, D. A. Krueger, R. Roble, P. Keckhut, A. Hauchecorne, and M. L. Chanin, Vertical structure of the mid-latitude temperature from stratosphere to mesopause (30-105 km), *Geophys. Res. Lett., 22,* 377-380, 1995.
Shibata, T., M. Kobuchi, and M. Maeda, Measurement of density and temperature profiles in the middle atmosphere with a XeF lidar, *Appl. Opt., 25,* 685-688, 1986.
Waters, J. W., Microwave limb sounding, in *Atmospheric Remote Sensing by Microwave Radiometry*, John Wiley, New York, 1993.
Whiteway, J. A., and A. I. Carswell, Rayleigh lidar observations of thermal structure and gravity wave activity in the high Arctic during a stratospheric warming, *J. Atmos. Sci., 51,* 3122-3136, 1994.
Whiteway, J. A., and A. I. Carswell, Lidar observations of gravity wave activity in the upper stratosphere over Toronto, *J. Geophys. Res., 100,* 14,113-14,124, 1995.
Whiteway, J. A., A. I. Carswell, and W. E. Ward, Mesospheric temperature inversions with overlying nearly adiabatic lapse rate: An indication of a well mixed turbulent layer, *Geophys. Res. Lett., 22,* 1201-1294, 1995.
Wickwar, V., T. D. Wilkerson, J. W. Meriwether, and D. Rees, The consortium lidar: Results, and facilities present and planned, paper presented at the Conference on Optical Remote Sensing of the Atmosphere, Opt. Soc. of Am., Salt Lake City, Feb. 5-9, 1995.

M. R. Gross and U. N. Singh (corresponding author), Hughes STX Corporation, Code 916, NASA/GSFC, Greenbelt, MD 20771. (e-mail: gross@aeolus.gsfc.nasa.gov; usingh@aeolus.gsfc.nasa.gov)

A. Hauchecorne and P. Keckhut, Service d'Aeronomie, CNRS, BP3, 91371 Verrières-le-Buisson, France. (e-mail: alain.hauchecorne@aerov.jussieu.fr; philippe.keckhut@aerov.jussieu.fr)

T. J. McGee, Laboratory for Atmospheres, code 916, NASA Goddard Space Flight Center, Greenbelt, MD 20771. (e-mail: mcgee@aeolus.gsfc.nasa.gov)

E. F. Fishbein and J. W. Waters, Jet Propulsion Laboratory, MS 183-701, Pasadena, CA 91109. (e-mail: eff@camel.jpl.nasa.gov; joe@mlsrac.jpl.nasa.gov)

J. C. Gille, National Center for Atmospheric Research, P.O. Box 3000, Boulder, CO 80307. (e-mail: gille@ncar.ucar.edu)

A. E. Roche, Lockheed Palo Alto Research Laboratory, Department 91-20, Palo Alto, CA 94304. (e-mail: roche@claes.space.lockheed.com)

J. M. Russell III, NASA Langley Research Center, MS 401B, Hampton, VA 23681. (e-mail: russell@larc.nasa.gov)

(Received October 18, 1995; revised February 7, 1996; accepted February 7, 1996.)